NUMERICAL ANALYSIS OF NATURAL CONVECTION IN TWO-DIMENSIONAL SQUARE AND CIRCULAR CONTAINERS IN LOW GRAVITY

August 1980

Contract NASW-3281   (Interim Report)

Prepared for

NASA HEADQUARTERS
WASHINGTON, DC   20546

by

S. J. Robertson
L. W. Spradley
M. P. Goldstein

Lockheed Missiles & Space Company, Inc.
Huntsville Research & Engineering Center
4800 Bradford Drive, Huntsville, AL 35807

FOREWORD

This document reports the results of effort by personnel of Lockheed Missiles & Space Company, Inc., Huntsville Research & Engineering Center, for the National Aeronautics and Space Administration under Contract NASW-3281, "Manufacturing in Space: Fluid Dynamics Numerical Analysis." The NASA technical director for this contract is Dr. Robert F. Dressler, Manager, Advanced Technology Program, NASA Headquarters, Washington, D. C.

ACKNOWLEDGMENT

The authors are pleased to express appreciation to the NASA technical director, Dr. Robert F. Dressler, and the originator of the effort, Dr. John R. Carruthers, for their interest in and support for this work. Dr. Dressler's guidance and monitoring of our efforts contributed substantially to the outcome of this task.

We are also grateful to Lockheed personnel who contributed in various ways to this effort, in particular, Kenneth E. Xiques who made substantial contributions to the numerical computational work.

ABSTRACT

A numerical study of natural convection in circular cylinder and square enclosures shows that the analytic low Rayleigh number theory of previous investigators is valid for Rayleigh numbers up to 1000. For a Rayleigh number of 5000, steady state values of maximum fluid velocity differ by 20 percent. This deviation between analytic theory and numerical results increases for higher Rayleigh numbers. In addition, the low Rayleigh number theory is shown to be valid for higher Rayleigh numbers for a portion of the transient phase before significant deviation becomes apparent. It is also shown that square shaped experiment configurations may be analytically approximated with good accuracy by circular cylinders of equal cross sectional area for the prediction of convection velocities and flow patterns at low Rayleigh number.

CONTENTS

LIST OF ILLUSTRATIONS

NOMENCLATURE

Symbol	Description
d	cylinder diameter = 2 R
g	gravity force
L	length of square side
r	radial distance
R	cylinder radius
Ra	Rayleigh number $= \dfrac{g\beta \Delta T\, d^3}{\nu\alpha}$, cylinder $= \dfrac{g\beta \Delta T\, L^3}{\nu\alpha}$, square
T	temperature
T_o	initial mid-point temperature
ΔT	temperature difference across circular cylinder or square enclosure
t	time
$\tilde{t}$	dimensionless time $= \nu t/R^2$, cylinder $\nu t/(L/2)^2$, square
v	velocity
$\tilde{v}$	dimensionless velocity $= \dfrac{128\nu}{g\beta \Delta T\, d^2}\, v$, cylinder $= \dfrac{128\nu}{g\beta \Delta T\, (L)^2}\, v$, square
x, y	rectangular coordinates (Figs. 1 and 9)
α	thermal diffusivity
β	volumetric coefficient of thermal expansion

θ	polar angle (Fig. 1)
ν	kinematic viscosity
ψ	stream function
$\widetilde{\psi}$	dimensionless stream function $= \dfrac{128\nu}{g\beta\,\Delta T\,d^3}\,\psi$, cylinder
	$= \dfrac{128\nu}{g\,\beta\,\Delta T\,L^3}\,\psi$, square

vii

1. INTRODUCTION

The NASA Materials Processing in Space program includes a number of experiments to be performed using the Fluids Experiment System (FES) facility aboard the Spacelab vehicle in orbit. These experiments will investigate various fluid phenomena of interest to materials processing in space applications. Fluid convection induced by residual gravity forces under orbital conditions is of interest to a number of possible materials processing applications.

This report describes numerical fluid dynamics analyses of simplified geometries to investigate fluid convection behavior under various conditions of thermal gradients and gravitational loading. These combined effects are indicated by the magnitude of the Rayleigh number (see Nomenclature).

The particular configurations investigated in this study were two-dimensional circular cylinder and square enclosures with horizontally imposed initial temperature gradients. The fluid was water in both cases. Batchelor (Ref. 1) investigated rectangular enclosures using non-numerical analytical methods for the limiting case of low Rayleigh number (Ra → 0) and steady state conditions. Weinbaum (Ref. 2) made a similar study for the circular cylinder. Dr. Robert F. Dressler (Ref. 3) of NASA Headquarters has recently developed a non-numerical transient solution for the cylinder configuration.

The purpose of the numerical study described herein is to establish the range of Rayleigh numbers for which the low Rayleigh number theories of Batchelor, Weinbaum and Dressler may be considered valid. We used the Lockheed developed LOCAP (LOckheed Convection Analyzer Program) and GIM (General Interpolant Method) codes to perform these numerical

computations. The LOCAP code is a two-dimensional code for analyzing
convection in rectangular enclosures, and the GIM code is a general purpose
fluid mechanics code for all kinds of geometries and flow conditions. The
LOCAP computations were performed on the NASA-MSFC Univac 1108 com-
puter, and the GIM code on the much faster and more efficient NASA-Langley
STAR-100 vector computer.

2

2.   CIRCULAR CYLINDER ENCLOSURE

Numerical computations were made for natural convection within the circular cylinder configuration shown in Fig. 1.
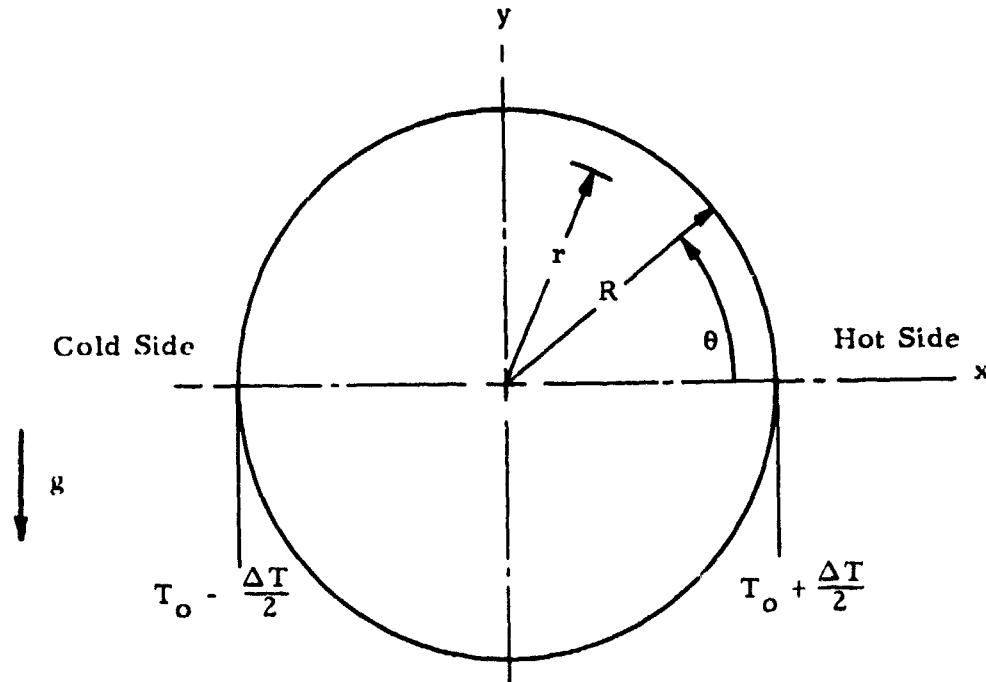

Fig. 1 - Geometry for Circular Cylinder Enclosure

The initial temperature distribution w is based on a horizontal gradient in the x direction, with the boundary points held constant in time:

$$T(r, o) = T_o + (\Delta T/2)\, x/R$$

$$T(R, t) = T_o + (\Delta T/2)\, \cos\theta \tag{1}$$

3

The geometry module of the GIM code divided the circular region into an array of 20 x 20 area elements with 21 x 21 nodal points. The process treated the boundary as a four-sided figure, each side being a circular arc. By use of stretching functions, each area element became a quadrilateral, with curvilinear sides, and with the nodal points located at its four corners. From the discussion of the computer generated velocity vector plots, it will become clear where the nodal points were placed.

We obtained transient flowfield computations over a range of Rayleigh numbers from 1 to 100,000. Figure 2a shows a time history of maximum computed flowfield velocities for various Rayleigh numbers. Both velocity and time are dimensionless as described in the nomenclature.

Up through Ra = 1000, the values of $\tilde{v}_{max}$ closely follow the same curve through steady state. This curve is also close to the theoretical transient of Dressler (Ref. 3). Some deviation from the low Ra results begins to occur at $\tilde{t}$ = 0.1 for Ra = 5000 and 10,000. The steady state values for these cases were extrapolated from the derivatives of $\tilde{v}_{max}$, since the numerical calculations converged slowly.

For higher Ra the deviations begin at earlier times. Thus, for Ra = 100,000, the low Ra curve is followed until $\tilde{t}$ = 0.06 where $\tilde{v}_{max}$ peaks and then falls to a lower steady state value. Figure 2b shows a time history of $\tilde{v}_{max}$ deviation from the low Ra values. For Ra = 5000, the deviation is less than 2% throughout the transient phase, while for Ra = 10,000 this level is reached halfway through the transient. For the higher Rayleigh numbers, 20% deviation is reached about one-third through the transient period.

Figure 3 shows $\tilde{v}_{max}$ at steady state as a function of Ra. The computed results closely approach the analytic value for low Ra, showing that the theory is valid up to Ra = 1000. The range of values 5000 < Ra < 50,000 may be viewed as a "transition" region. For larger Ra, the trend in $\tilde{v}_{max}$ approaches the $(Ra)^{-\frac{1}{2}}$ dependence given by Weinbaum (Ref. 2).

4
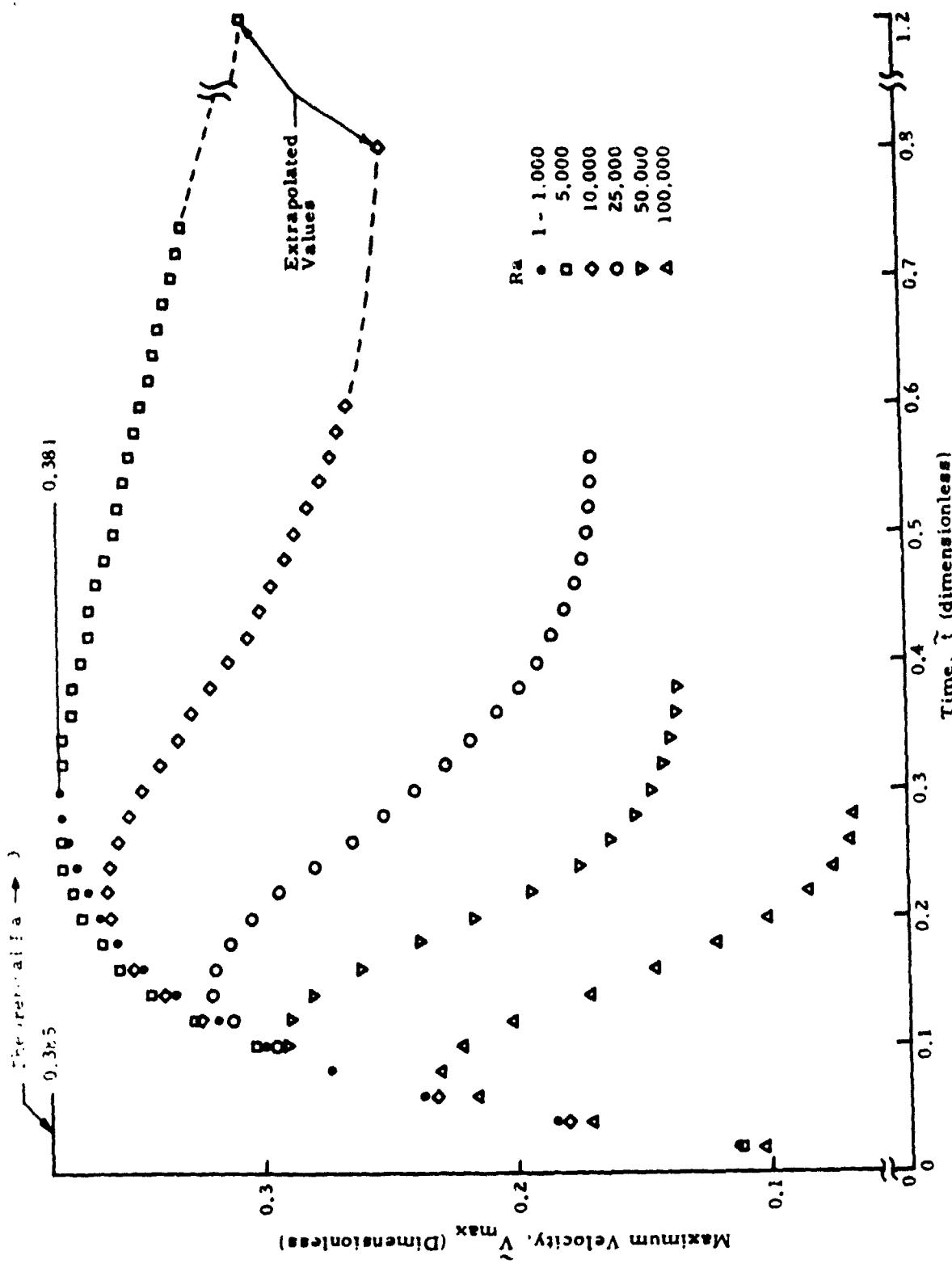
Fig. 2a — Maximum Velocity as a 'ion of Time for Water Contained in a Horizontal Circular Cylinder Enclu at Various Rayleigh Numbers
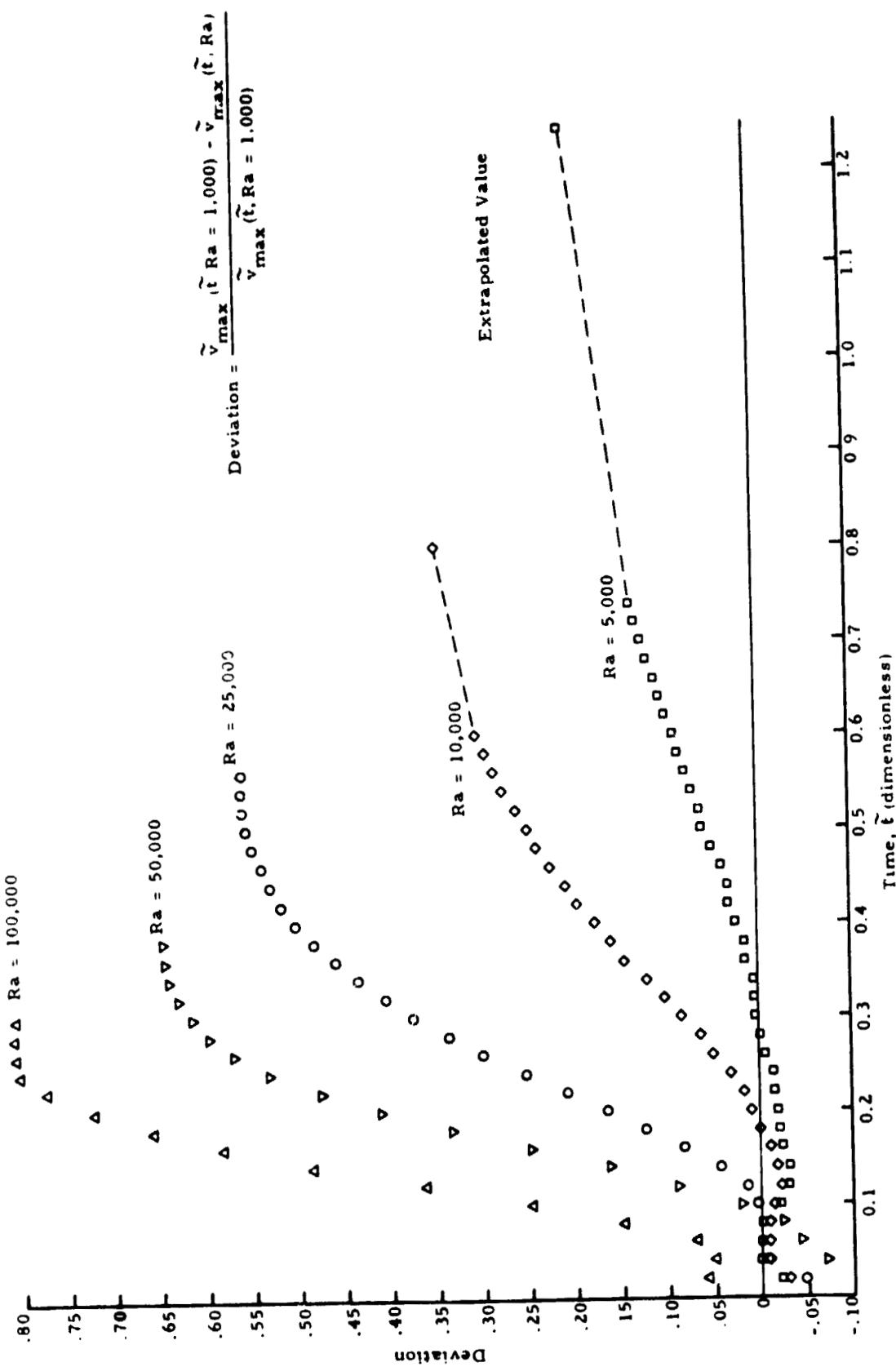
Fig. 2b - Velocity Deviation as a Function of Time for Water Contained in a Horizontal Circular Cylinder Enclosure at Various Rayleigh Numbers

6
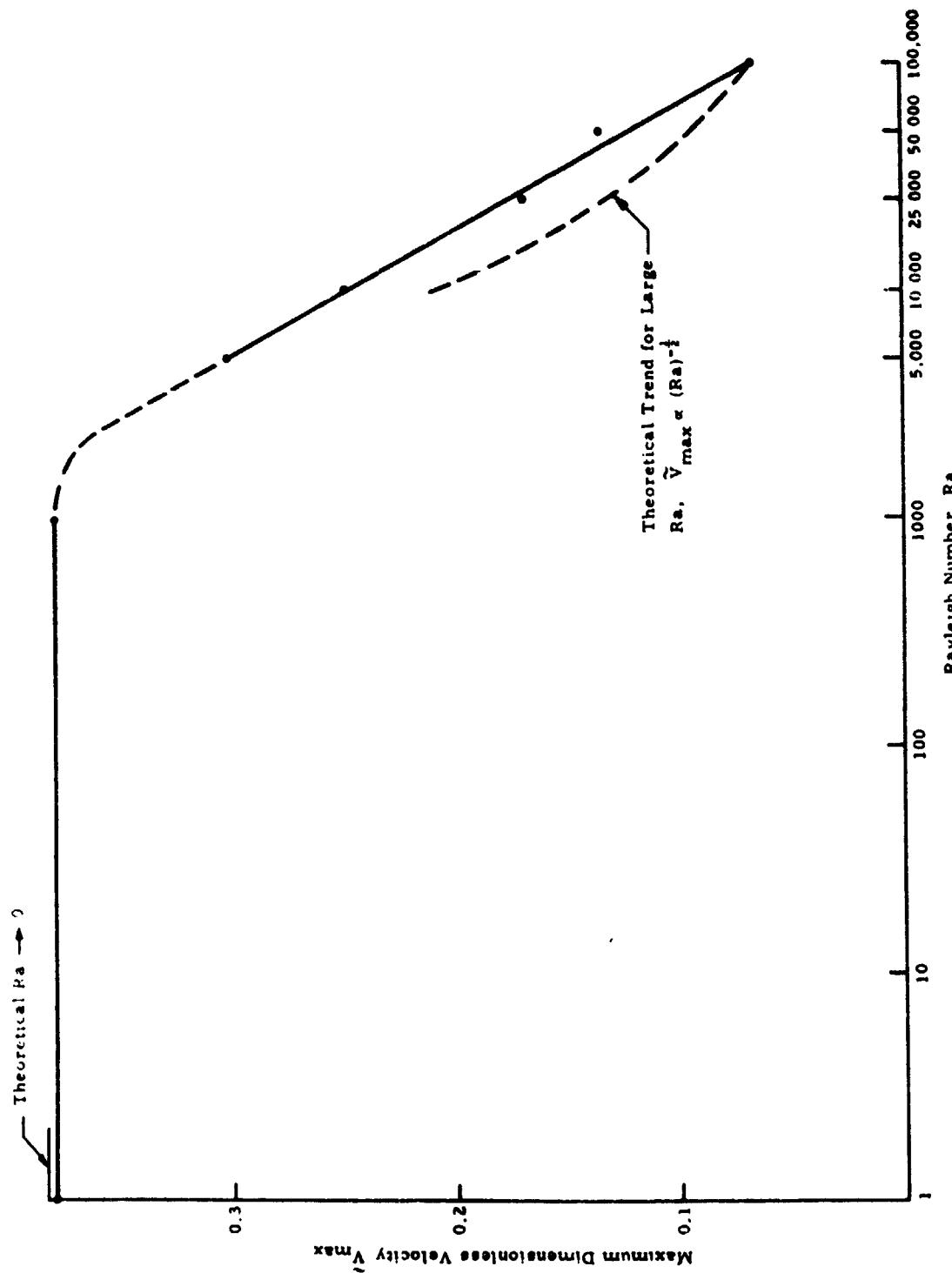
Fig. 3 – Variation of Maximum Equilibrium Velocity with Rayleigh Number for Water Contained in a Horizontal Cylinder

7

The low Ra theory is also valid for higher Ra during some initial part of the transient. As noted earlier, for Ra = 100,000 this initial stage last until $\tilde{t}$ = 0.06. This is further indicated by comparison of the radial distribution of velocities for Ra = 1 and 100,000 shown in Fig. 4. Not only the maximum velocity, but also the entire velocity field compares well up to $\tilde{t}$ = 0.06. Note that the computed distribution approaches the low Ra theoretical steady state distribution. Note also that the early velocity distributions are essentially linear for a considerable distance away from the center, thus forming a solid body rotation inner core that gradually diminishes with time.

GIM code generated velocity vector plots reveal that the flow at low Raleigh number remains unicellular from initial transient through steady state. The velocity vector plot shown in Fig. 5 for Ra = 1 at steady state is seen to be nearly perfectly circular. This plot is essentially duplicated throughout the transient phase for all Rayleigh numbers up through Ra = 1,000. A slight distortion in the circular flow pattern is seen for Ra = 10,000, and a distinct breakup into multiple cells is noted for Ra = 100,000. This departure from circular flow is also indicated by the velocity contour plots in Fig. 6. Note the skewness that has developed in the still unicellular contours for Ra = 10,000. This skewness is apparently carried over into the multiple cell contours for Ra = 100,000.

Heat transfer at low Rayleigh numbers is dominated by conduction, and the effect of increasing Rayleigh number is to increase the distortion of the temperature contours from the initial conduction profile. This effect is shown in the steady state temperature contour plots in Fig. 7. Note that for Ra = 1 the contours are nearly straight lines, corresponding to a nearly pure conduction temperature field. The distortion in the temperature field at higher Rayleigh numbers leads to an unstable condition that results in departure from circular flow and, for sufficiently high Rayleigh numbers, eventual breakup into multiple cells. This is clearly indicated in the comparison of temperature contour and velocity vector plots shown in Fig. 8 for various times with Ra = 100,000. At $\tilde{t}$ = 0.1, the temperature field is greatly distorted from the initial pure conduction

8
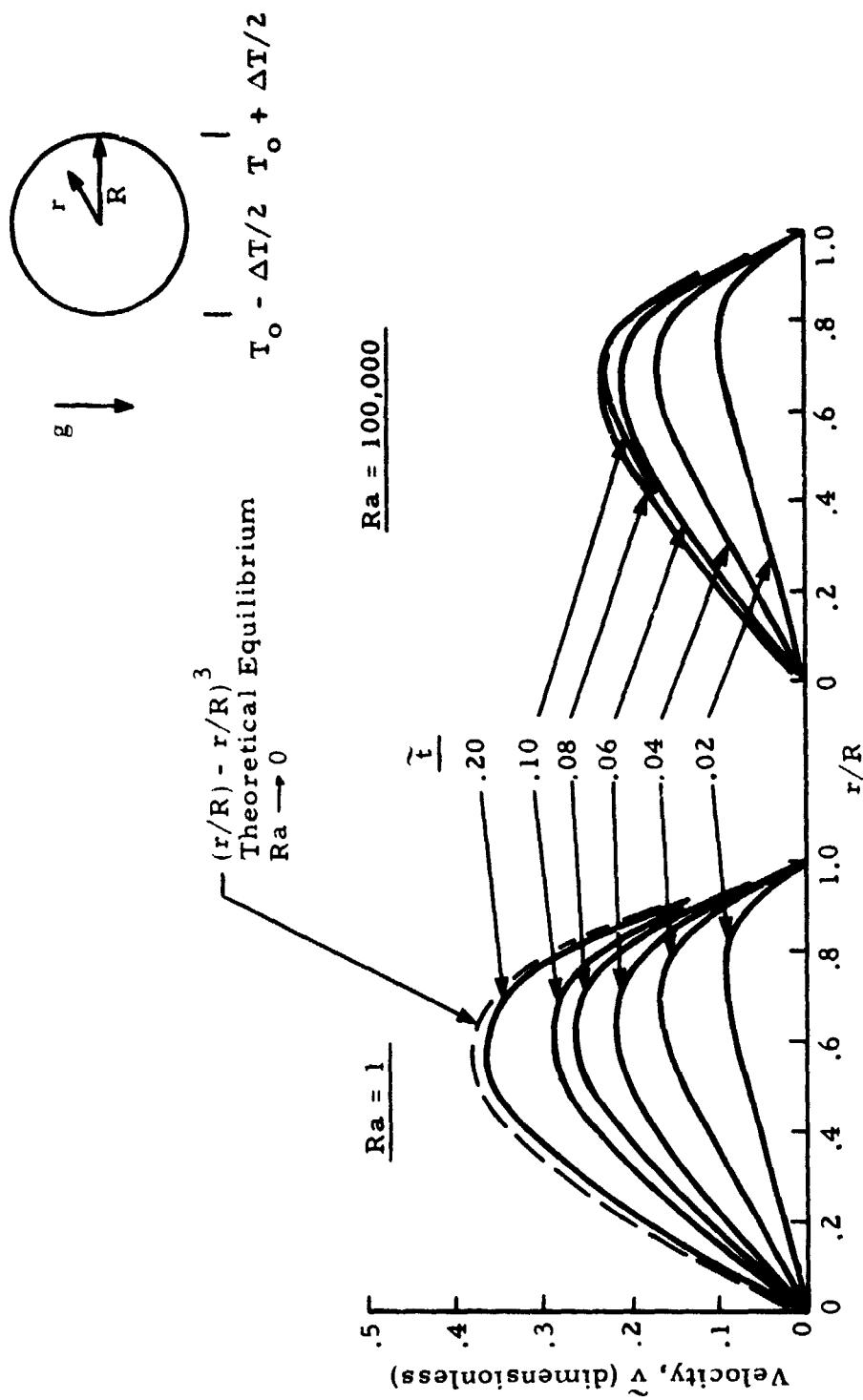
Fig. 4 - Comparison of Velocity Distributions Along Horizontal Radius as a Function of Time for Rayleigh Numbers of 1 and 100,000
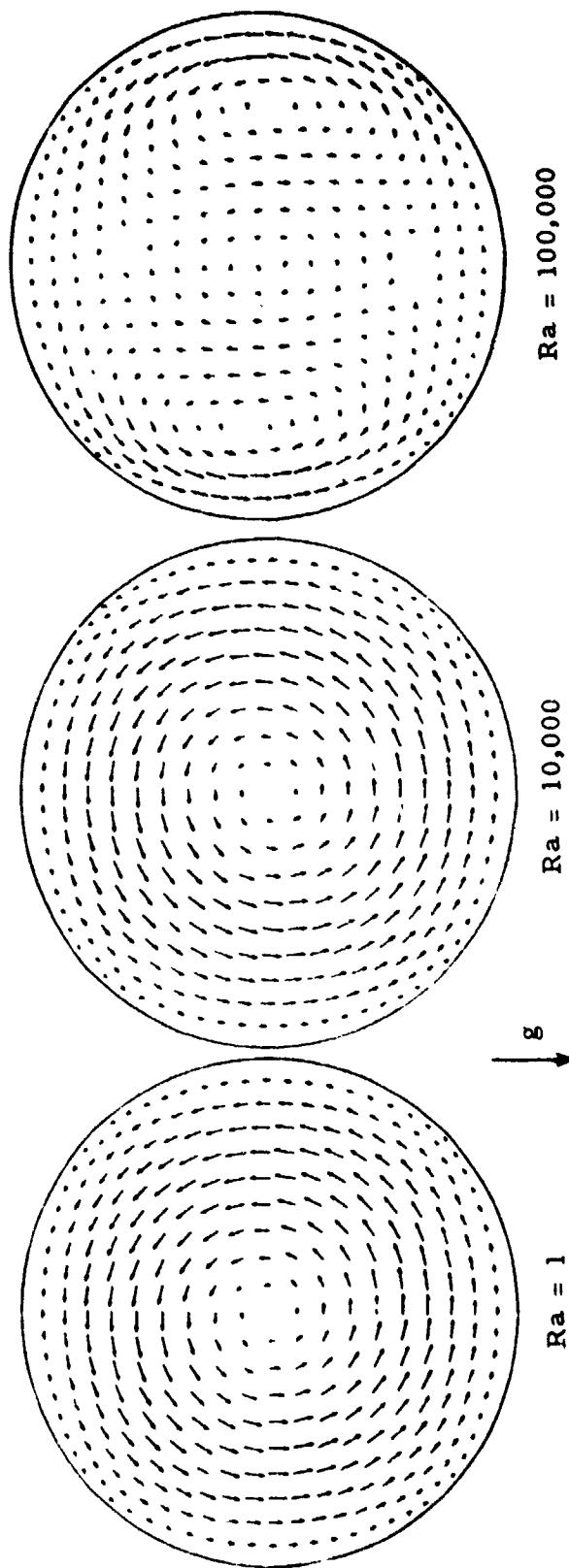
Ra = 100,000

Ra = 10,000

Ra = 1

g

Fig. 5 - GIM Code Velocity Vector Plots at Steady State for Circular Cylinder at Various Rayleigh Numbers

	1	2	3	4	5	6	7	8	9	10
$\tilde{v}/\tilde{v}_{max}$	.05	.15	.25	.35	.45	.55	.65	.75	.85	.95

Ra	$\tilde{v}_{max}$
1	.385
10,000	.349
100,000	.0669

Ra = 100,000

Ra = 10,000

g →

Ra = 1

Fig. 6 - GIM Code Velocity Contour Plots at Steady State for Circular Cylinder at Various Rayleigh Numbers

11

$\frac{T-T_o}{\Delta T}$	1	2	3	4	5	6	7	8	9	10
	-.45	-.35	-.25	-.15	-.05	.05	.15	.25	.35	.45
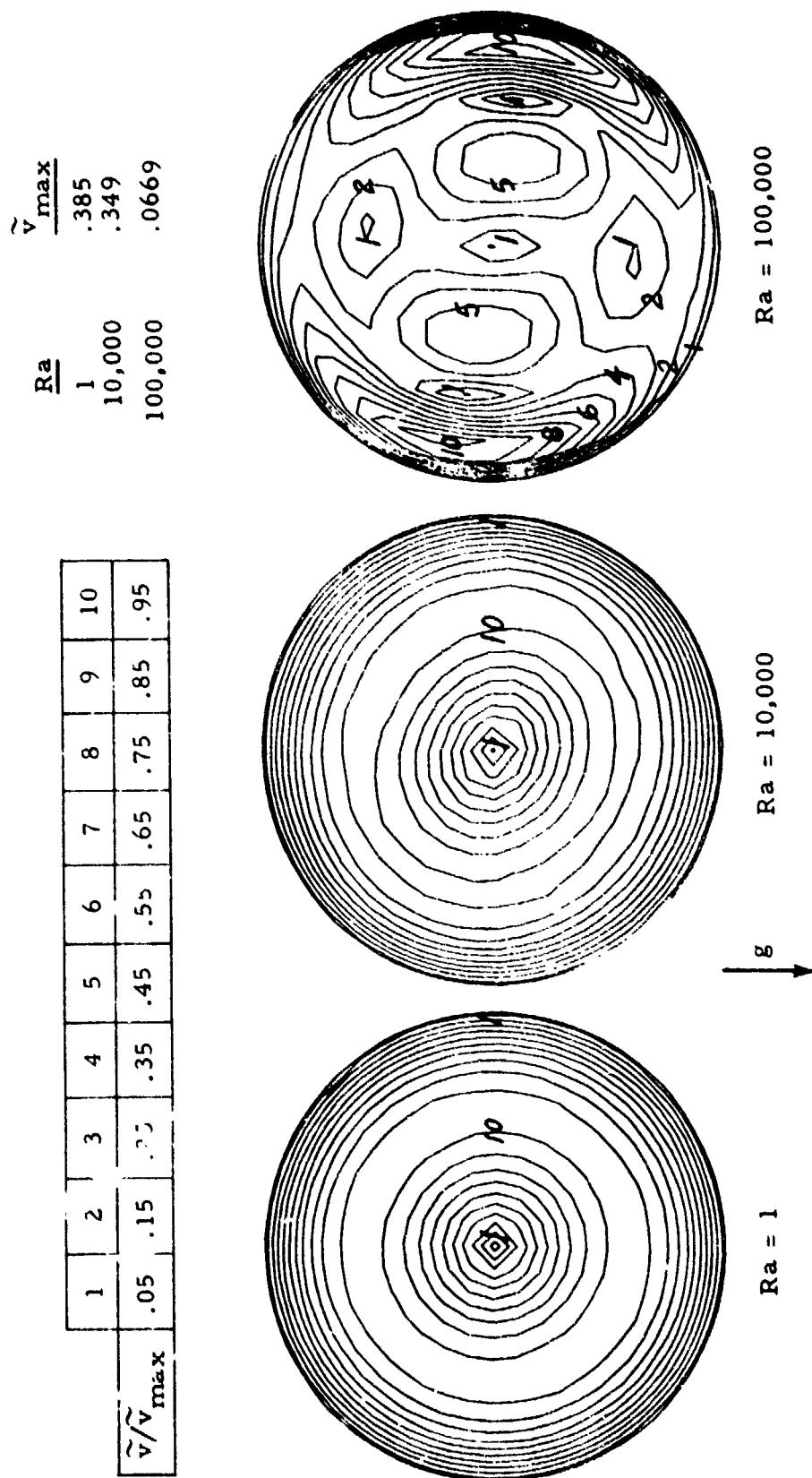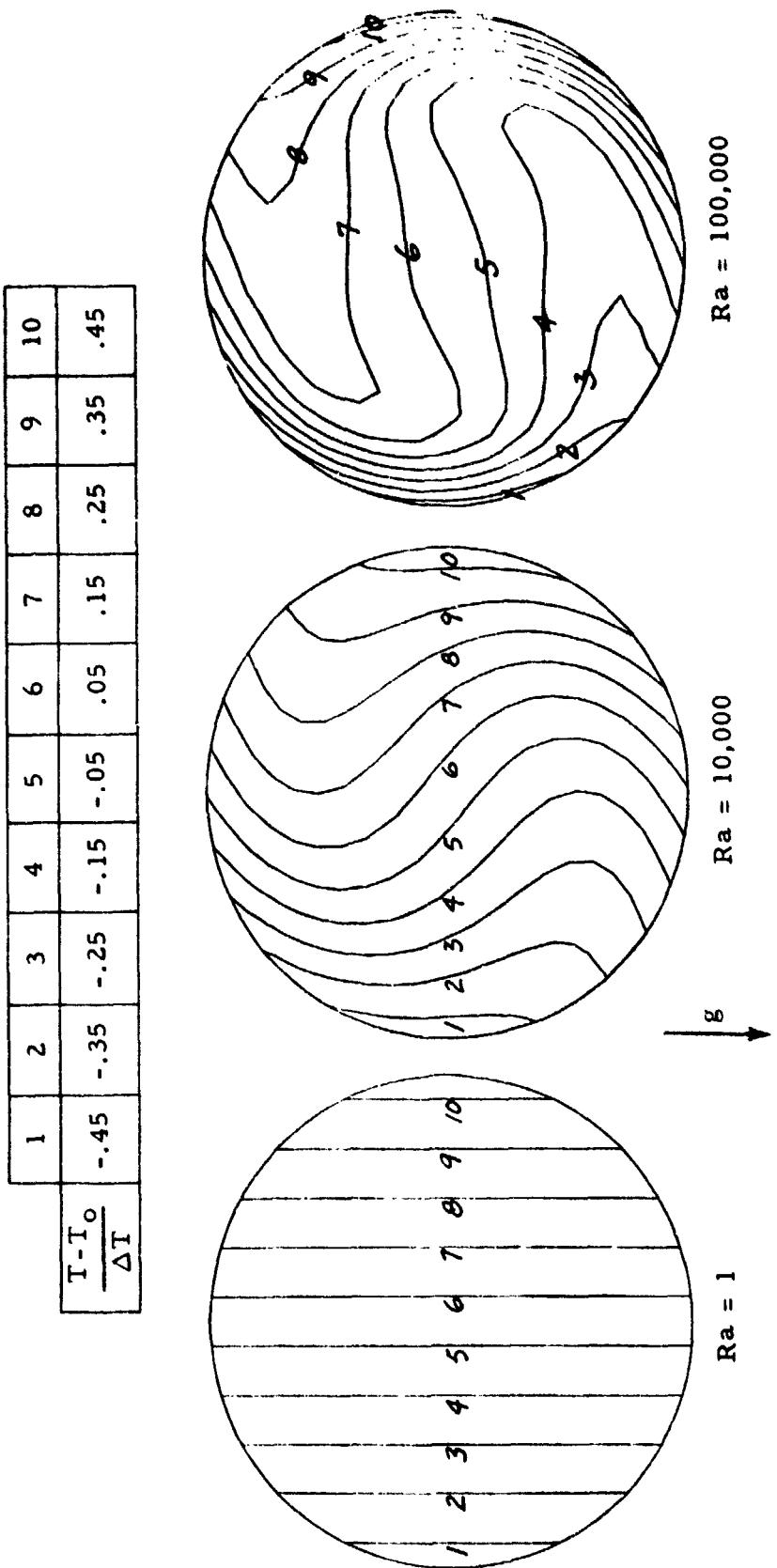
Fig. 7 - GIM Code Temperature Contour Plots at Steady State for Circular Cylinder at Various Rayleigh Numbers

12

Temperature Contours (See Fig. 7 for contour identification)
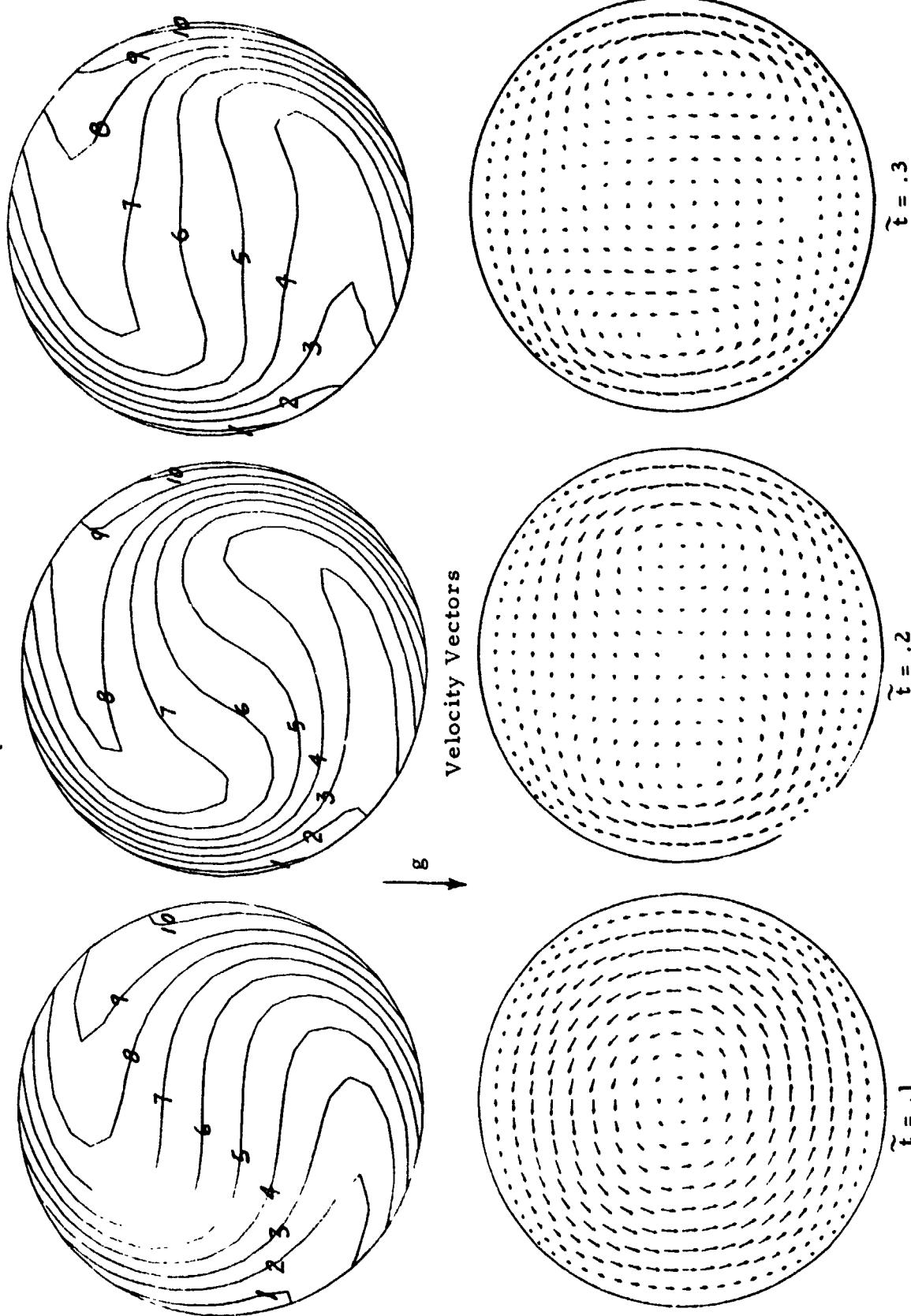
Velocity Vectors

Fig. 8 - Comparison of GIM Code Temperature Contour and Velocity Vector Variation with Time for Circular Cylinder at Rayleigh Number of 100,000

13

field, with the interior contours nearly horizontal. The flow is still uni-cellular, but it has become somewhat skewed. By $\tilde{t} = 0.2$, the flow has broken up into two cells, and this has caused the temperature contours to loop past the horizontal and to further distort the temperature field. By $\tilde{t} = 0.3$, a third cell has developed and this has tended to shift the tempera-ture contours back toward a more stable configuration.

14

3. SQUARE ENCLOSURE

The square enclosure configuration is illustrated in Fig. 9.
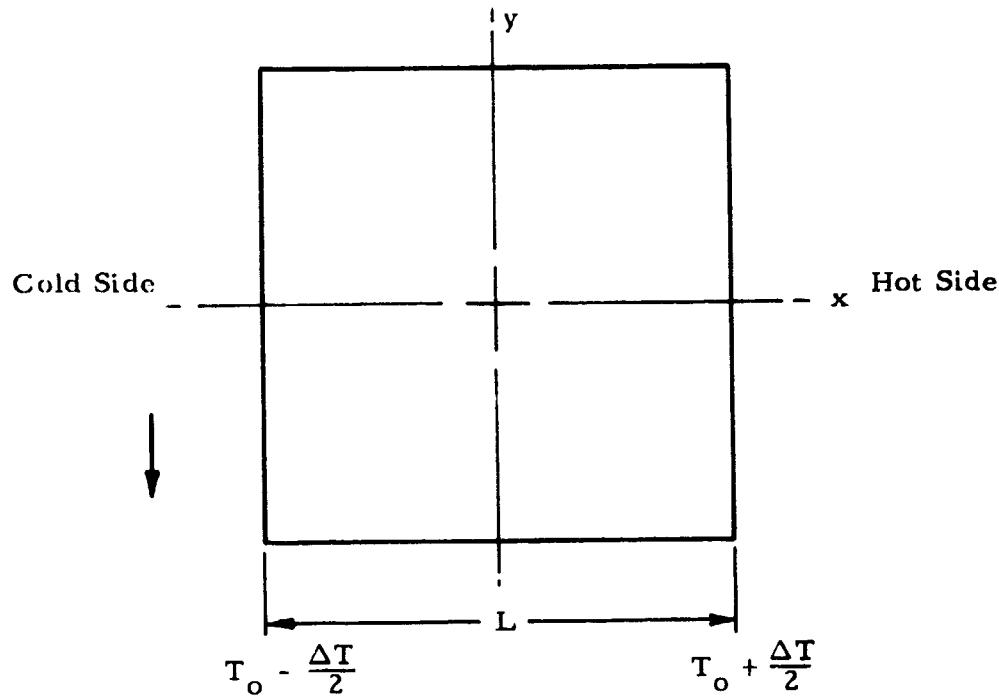
Fig. 9 - Geometry for Square Enclosure

Numerical computations were made with the LOCAP code using a 10 x 10 array of square elements and the GIM code using a 20 x 20 array. The LOCAP code was used to get initial results because it had existing capability for considering buoyarcy effects. The GIM code was used later after modifications were made to the program to include buoyancy. As in the circular cylinder, the initial temperature distribution was based on a horizontal gradient in the x direction. Calculations were made using the LOCAP code for both adiabatic (zero normal temperature gradient) and constant temperature boundary conditions on the top and bottom surfaces. The side surface temperatures were held constant in both cases. The GIM code calculations were for constant temperature boundaries only.

15

Shown in Fig. 10 are the computed maximum flow velocities as a function of Rayleigh number after the flow has reached an equilibrium condition. The theoretical low Rayleigh number limiting value, based on the first order stream function in Ref. 1, is shown for comparison. Good agreement is noted between the theoretical low Rayleigh number limit and the computed results. The LOCAP results indicate significant deviation from the low Rayleigh number results starting at about Ra = 1000. The GIM code results follow the same general trend, but the deviation occurs at higher Rayleigh number. Note that the adiabatic boundary produces the greatest deviation from the low Rayleigh number results in the LOCAP data.

LOCAP generated plots of velocity vectors, streamlines and absolute velocities are shown in Figs. 11, 12 and 13. Note the skewness that develops in the unicellular flow patterns as Rayleigh number increases. At Ra = 100,000, the flow appears to be nearly broken up into two cells. LOCAP plots of temperature contours are shown in Fig. 14. Note that the adiabatic boundary permits a greater distortion in the temperature contours than the constant temperature boundary. This probably accounts for the greater deviation from the low Rayleigh number results shown in Fig. 10 for the adiabatic boundary cases.

GIM code generated velocity vector, absolute velocity and temperature contour plots are shown in Figs. 15, 16 and 17 for constant temperature boundaries. The GIM code results generally confirm the LOCAP data. The GIM code, however, predicts a definite breakup into three convection cells at Ra = 100,000, whereas the LOCAP code noted only an apparent incipient double cell pattern at the same Rayleigh number.

The differences between the LOCAP and GIM results may be attributed not only to differences in the LOCAP and GIM computational techniques, but also to the fact that the GIM computations were based on finer grid of nodal points. The finer grid for the GIM computations was made possible by the greater speed and efficiency of the STAR-100 vector computer.

16
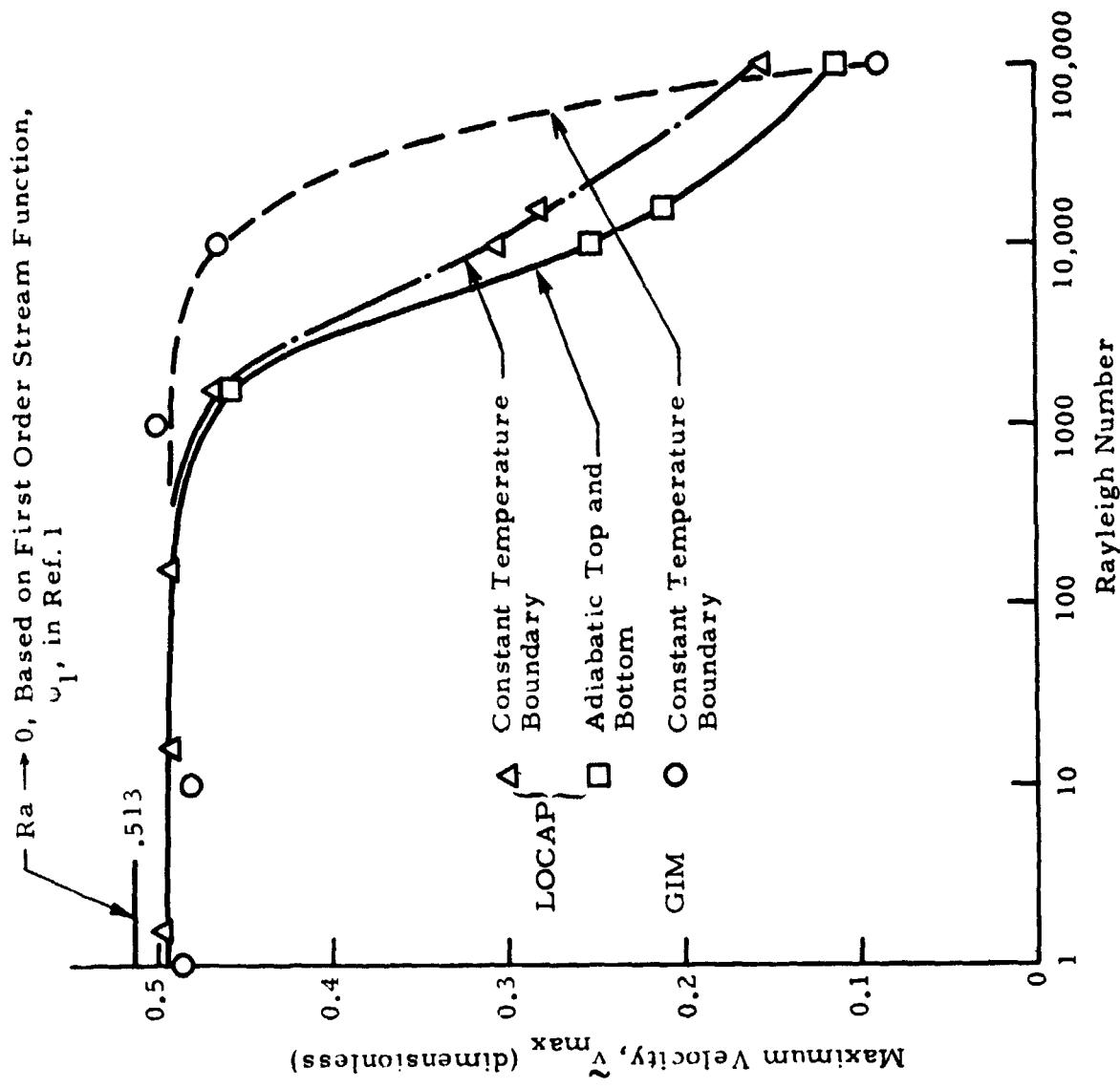
Fig. 10 - Variation of Maximum Equilibrium Velocity with Rayleigh Number for Water Contained in Square Enclosure

17
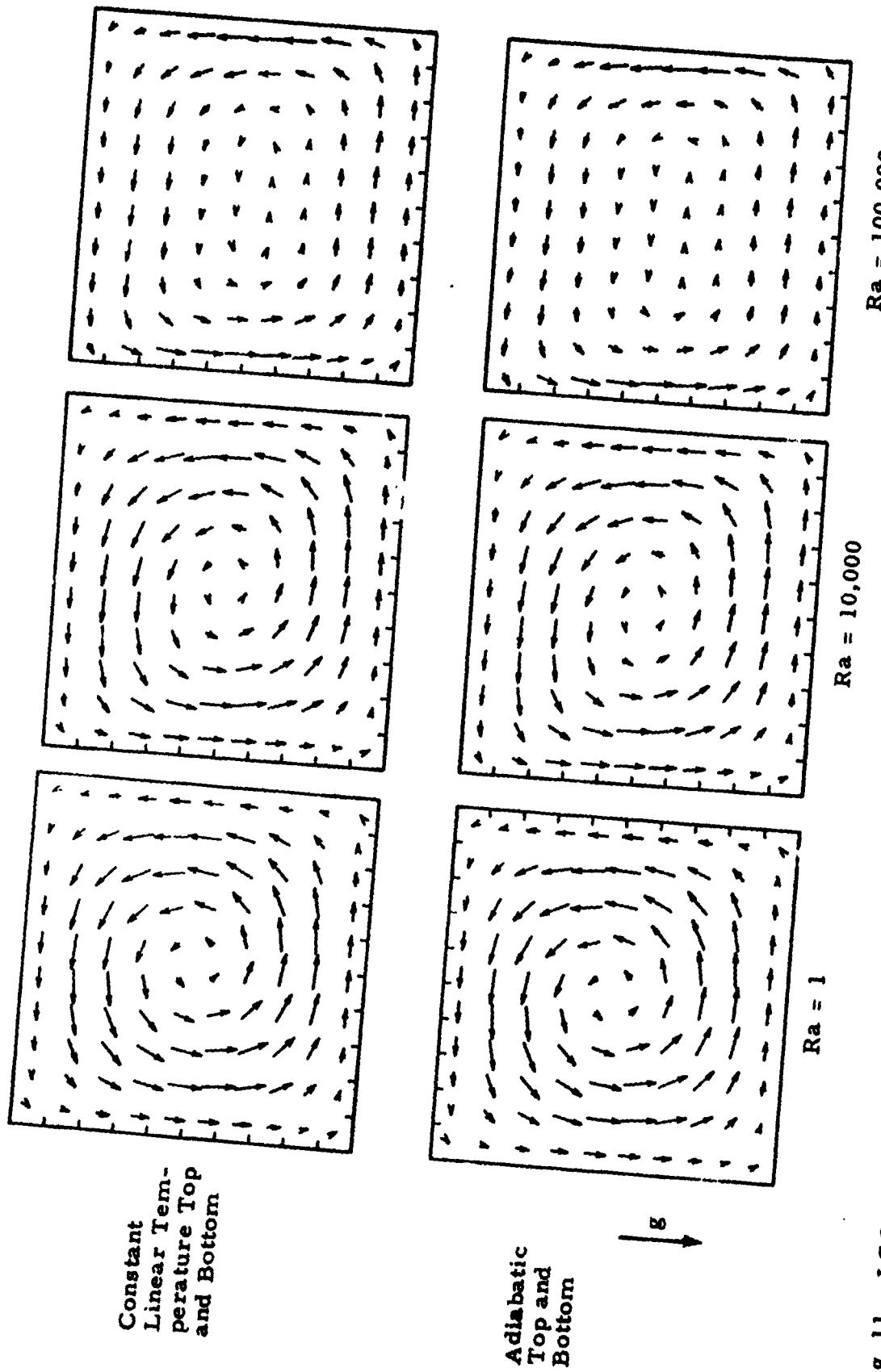
Fig. 11 - LOCAP Velocity Vector Plots at Steady State for Square Enclosure at Various Rayleigh Numbers

Ra = 100,000

Ra = 10,000

Ra = 1

Constant
Linear Tem-
perature Top
and Bottom

Adiabatic
Top and
Bottom

g

	1	2	3	4	5	6	7	8	9	10	11
$\tilde{\psi}/\tilde{\psi}_{max}$	.05	.1	.2	.3	.4	.5	.6	.7	.8	.9	.95

Constant Linear
Temperature
Top and Bottom

Ra	$\tilde{\psi}_{max}$
1	30.96
10,000	15.56
100,000	5.02

Adiabatic Top
and Bottom

Ra	$\tilde{\psi}_{max}$
1	30.96
10,000	12.47
100,000	3.11

Ra = 100,000

Ra = 10,000

Ra = 1
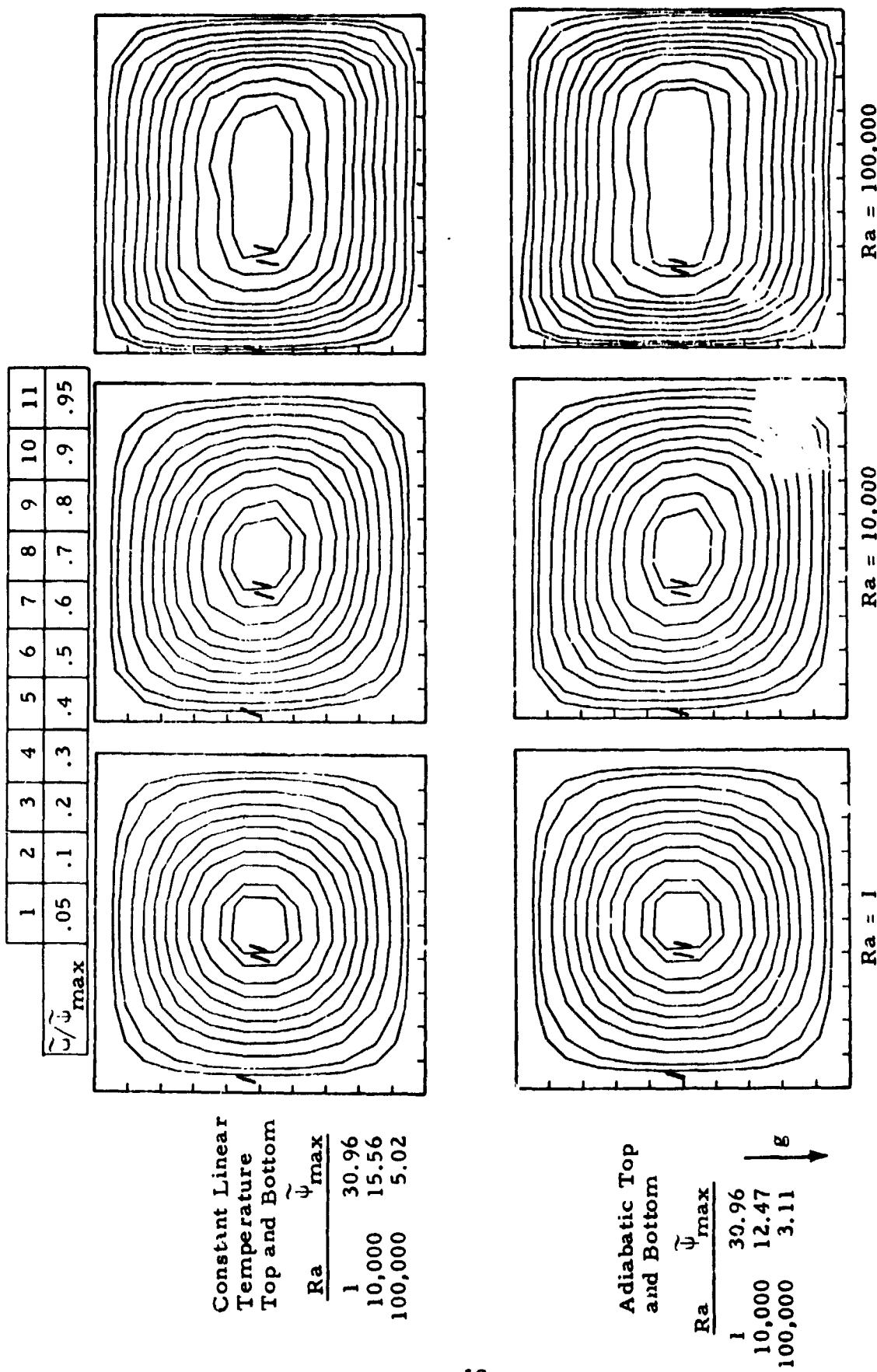
Fig. 12 - LOCAP Streamline Plots at Steady State for Square Enclosure at Various Rayleigh Numbers

19

	1	2	3	4	5	6	7	8	9	10	11
$\tilde{v}/\tilde{v}_{max}$	.05	.1	.2	.3	.4	.5	.6	.7	.8	.9	.95

Constant
Linear Tem-
perature Top
and Bottom

Ra	$\tilde{v}_{max}$
1	.497
10,000	.302
100,000	.156

Adiabatic Top
and Bottom

Ra	$\tilde{v}_{max}$
1	.497
10,000	.252
100,000	.114

Ra = 100,000

Ra = 10,000

Ra = 1
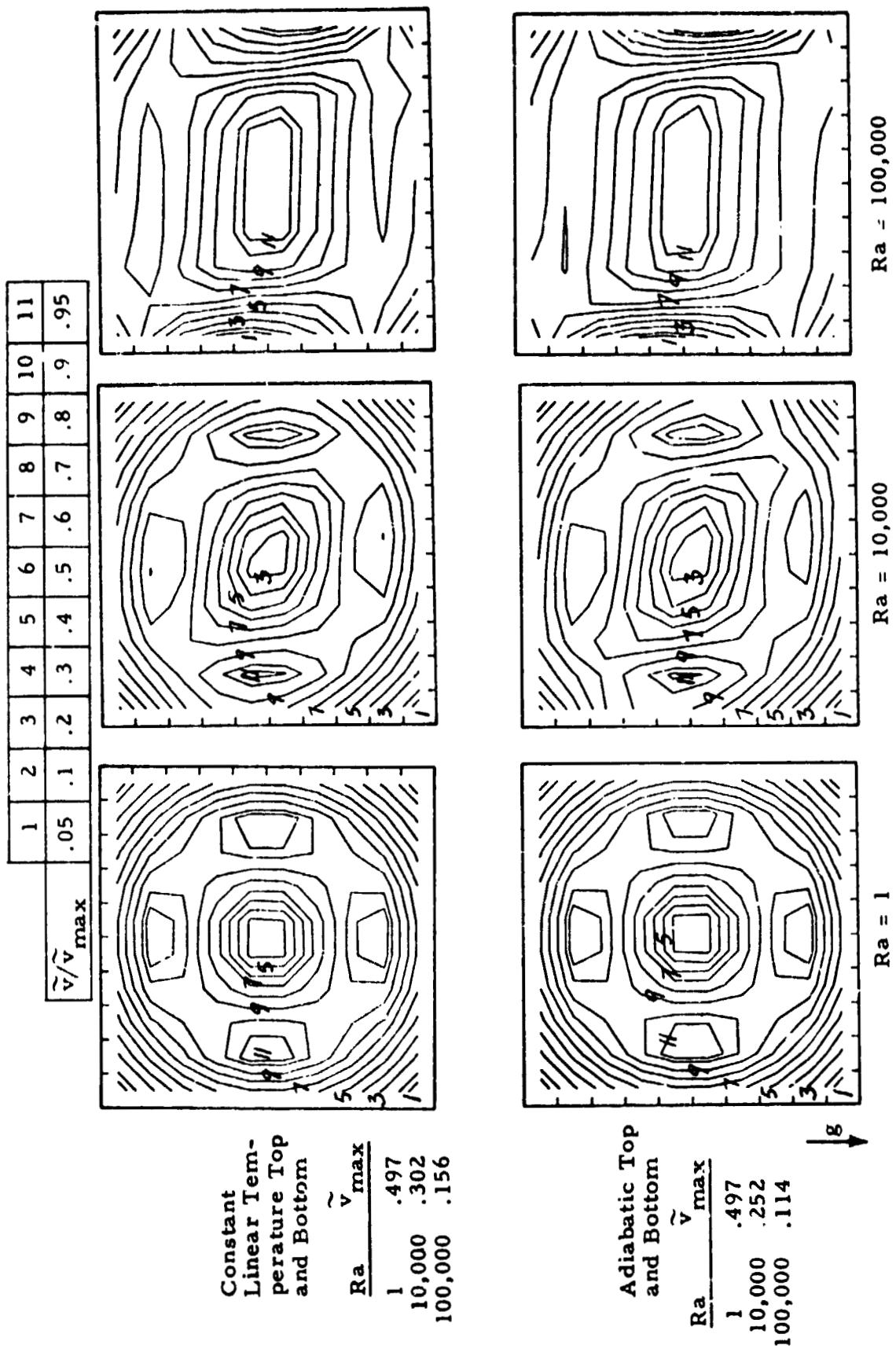
Fig. 13 - LOCAP Absolute Velocity Contour Plots at Steady State for Square Enclosure at Various Rayleigh Numbers

20

LOCKHEED - HUNTSVILLE RESEARCH & ENGINEERING CENTER
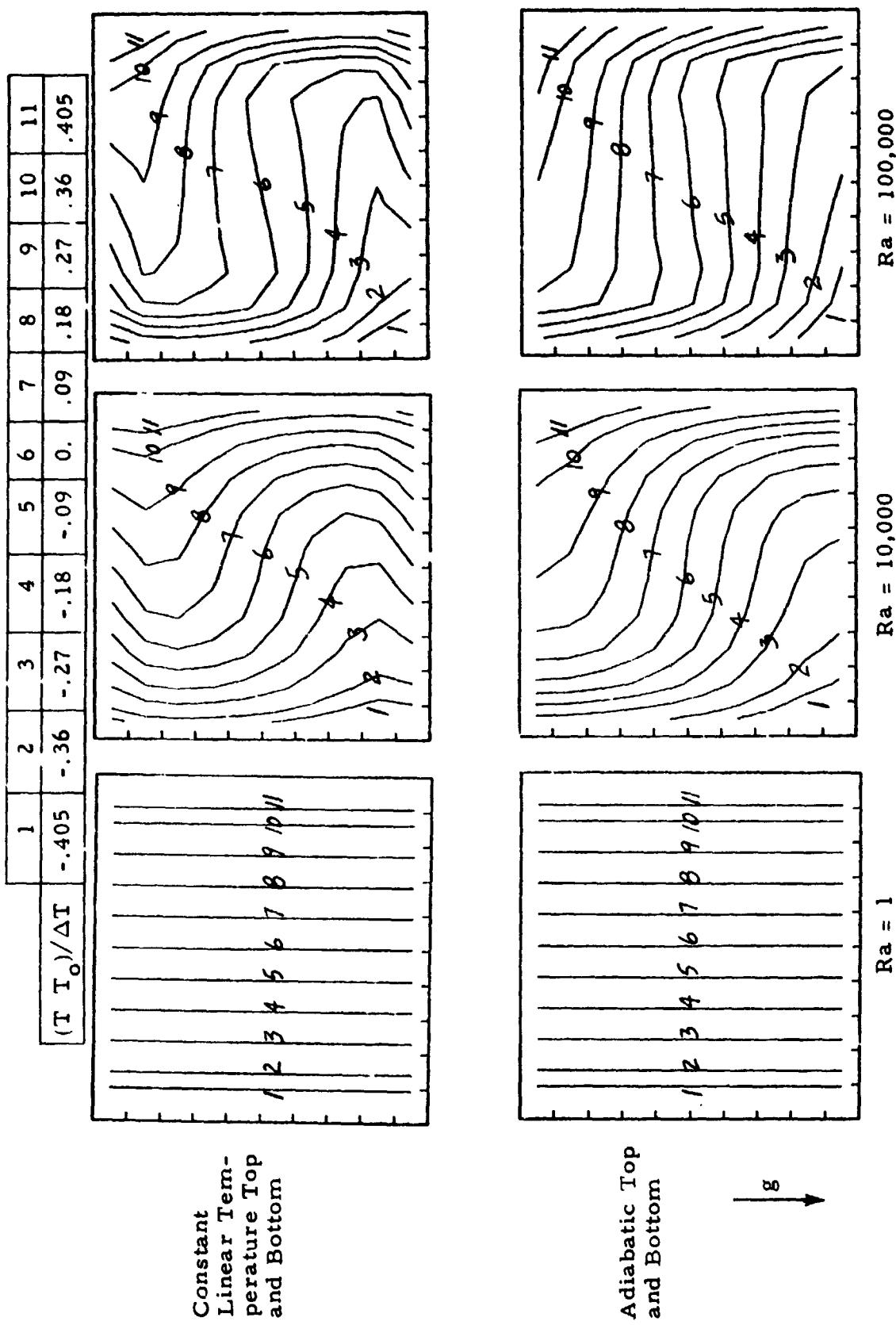
Fig. 14 – LOCAP Temperature Contour Plots at Steady State for Square Enclosure at Various Rayleigh Numbers

	1	2	3	4	5	6	7	8	9	10	11
$(T-T_o)/\Delta T$	-.405	-.36	-.27	-.18	-.09	0.	.09	.18	.27	.36	.405

Constant Linear Temperature Top and Bottom

Adiabatic Top and Bottom

Ra = 100,000

Ra = 10,000

Ra = 1

g →

21

Ra = 100,000

Ra = 10,000

Ra = 1

g

Fig. 15 - GIM Code Velocity Vector Plots at Steady State for Square Enclosure at Various Rayleigh Numbers

LOCKHEED - HUNTSVILLE RESEARCH & ENGINEERING CENTER

	1	2	3	4	5	6	7	8	9	10
$\tilde{v}/\tilde{v}_{max}$	.05	.15	.25	.35	.45	.55	.65	.75	.85	.95

| Ra	$\tilde{v}_{max}$
1	.487
10,000	.463
100,000	.0891

Ra = 100,000

Ra = 10,000

Ra = 1

g

Fig. 16 - GIM Code Velocity Contour Plots at Steady State for Square Enclosure at Various Rayleigh Numbers

23

Contour Labels same as Fig. 7

Ra = 1

Ra = 10,000

Ra = 100,000

Fig. 17 - GIM Code Temperature Contour Plots at Steady State for Square Enclosure at Various Rayleigh Numbers

24
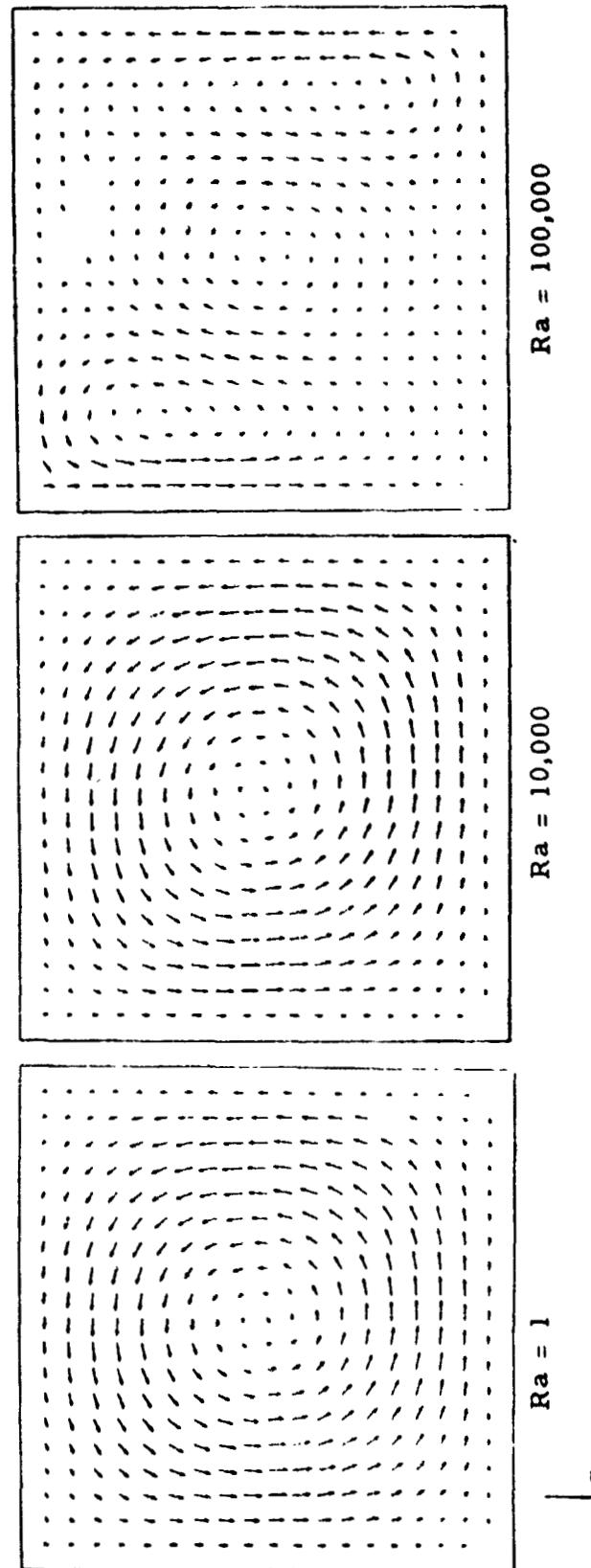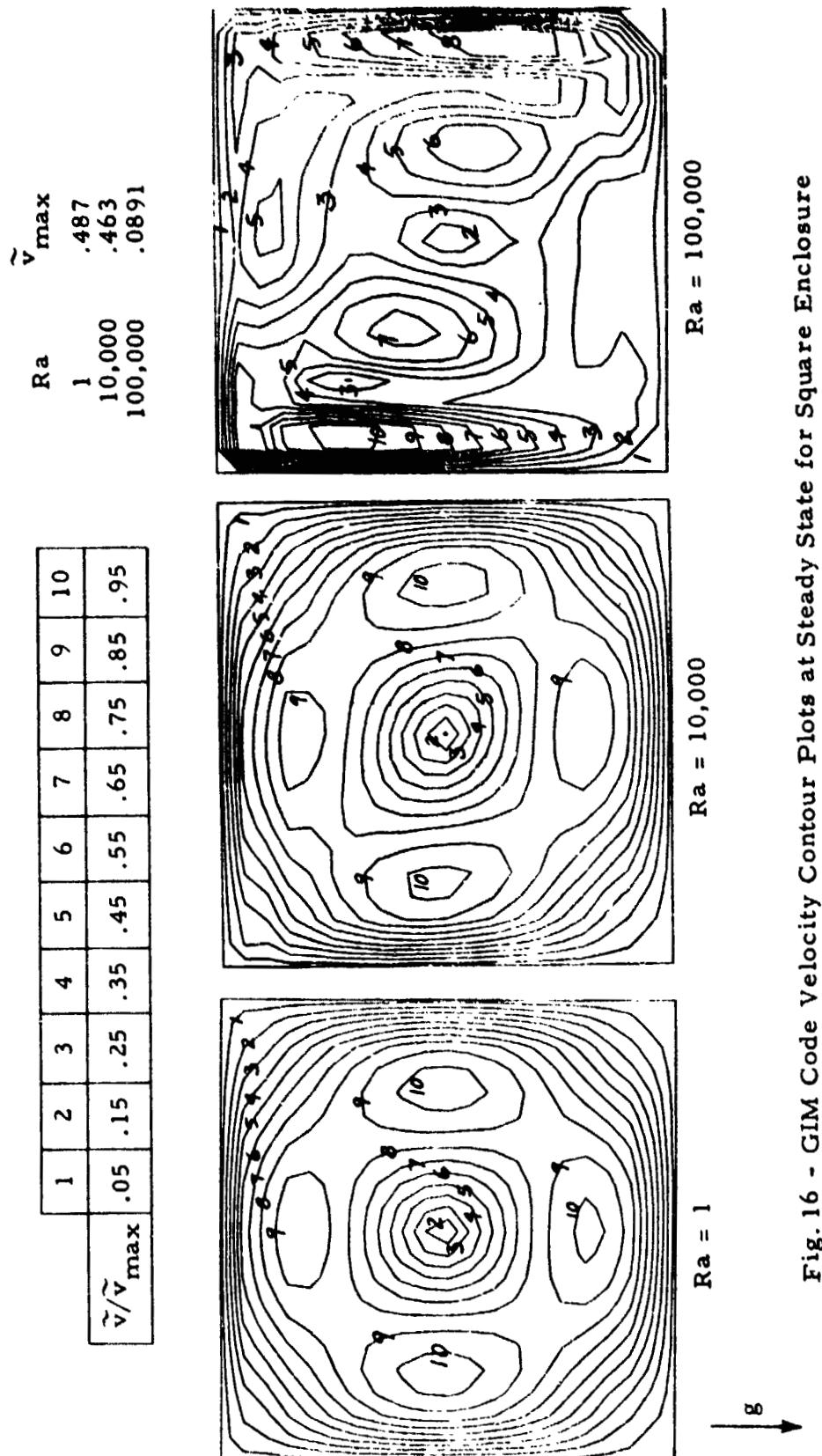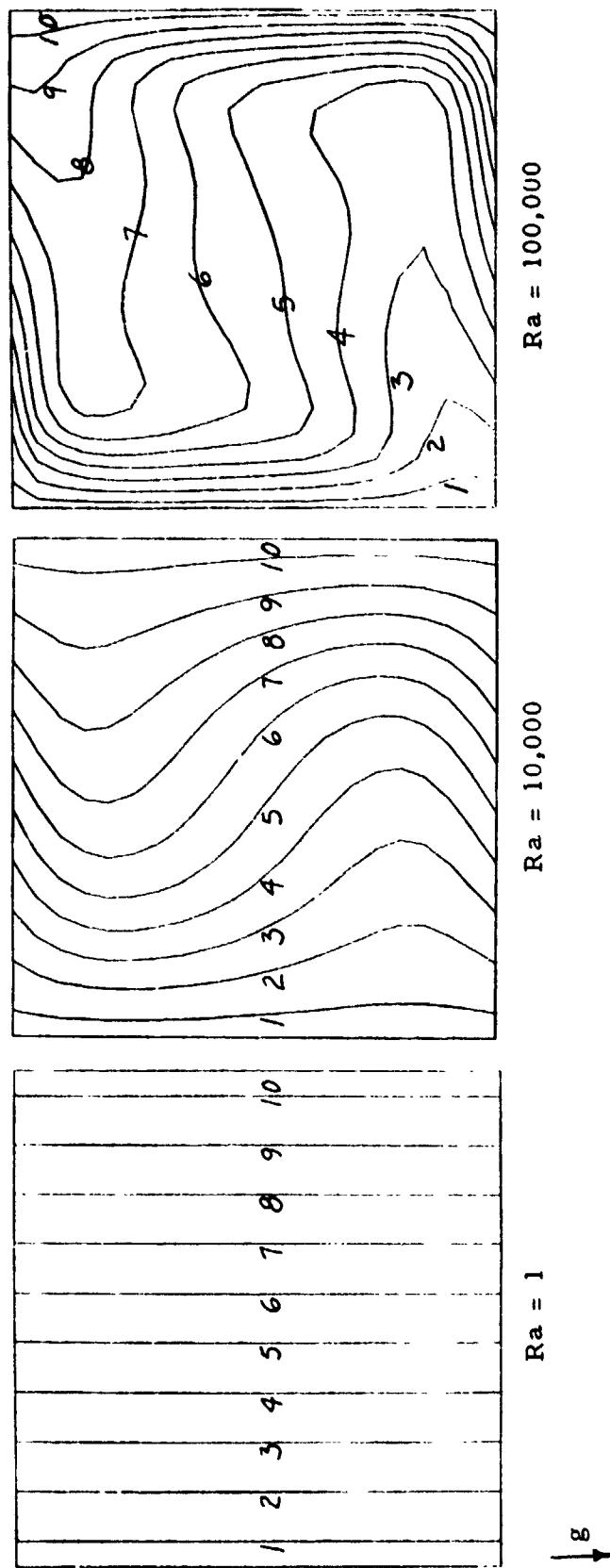
The variation in maximum velocity as a function of time is shown in Fig. 18 for the GIM code data. The LOCAP code did not provide realistic results during the transient phase for the lower Rayleigh numbers. The GIM code results in Fig. 18 exhibit basically the same trends noted earlier in Fig. 2 for the circular cylinder. Again, the theoretical low Rayleigh number limiting value, based on the first order stream function, ψ_1, in Ref. 1, is shown for comparison.

The velocity distribution along a horizontal bisector is shown in Fig. 19 as a function of time for Ra = 1. The low Rayleigh number theoretical equilibrium distribution is shown for comparison. The traversing of the theoretical equilibrium curve over the GIM code results near equilibrium for $x/(L/2) > 0.7$ is obviously not realistic. The solution for the first order stream function given by Batchelor in Ref. 1 is actually an approximate solution intended to provide a simple algebraic equation form for the stream function. Hence, exact agreement is not expected.

A comparison of temperature contour and velocity vector plots at various times is shown in Fig. 20 for Ra = 100,000. A strong correlation is indicated between distortion of the temperature field and departure from symmetrical unicellular flow, as was shown earlier in Fig. 8 for the circular cylinder.

A strong similarity has been noted throughout this section between the square enclosure and the previously discussed circular cylinder results. This suggests the possibility of using the simpler, more analytically defined circular cylinder theory to predict convection velocities and flow patterns in actual experiment configurations, which are more likely to be square than circular. In order to match velocities in a model circular cylinder configuration to an experimental square enclosure, we set the theoretical equilibrium velocities for the two configurations equal and find the ratio of the circle diameter to square side (page 29):

25
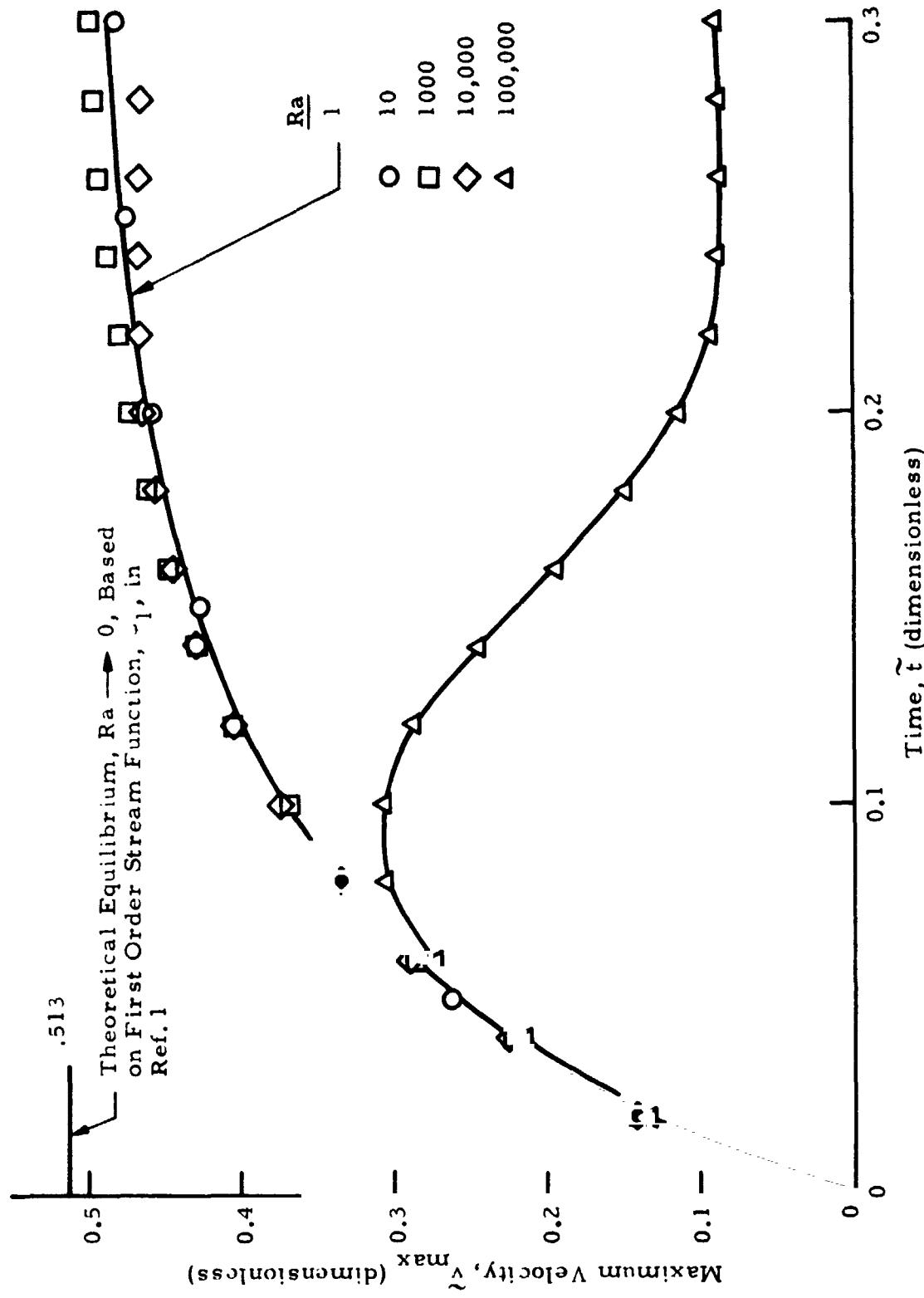
Fig. 18 - Maximum Velocity as a Function of Time for Water Contained in a Square Enclosure at Various Rayleigh Numbers

26
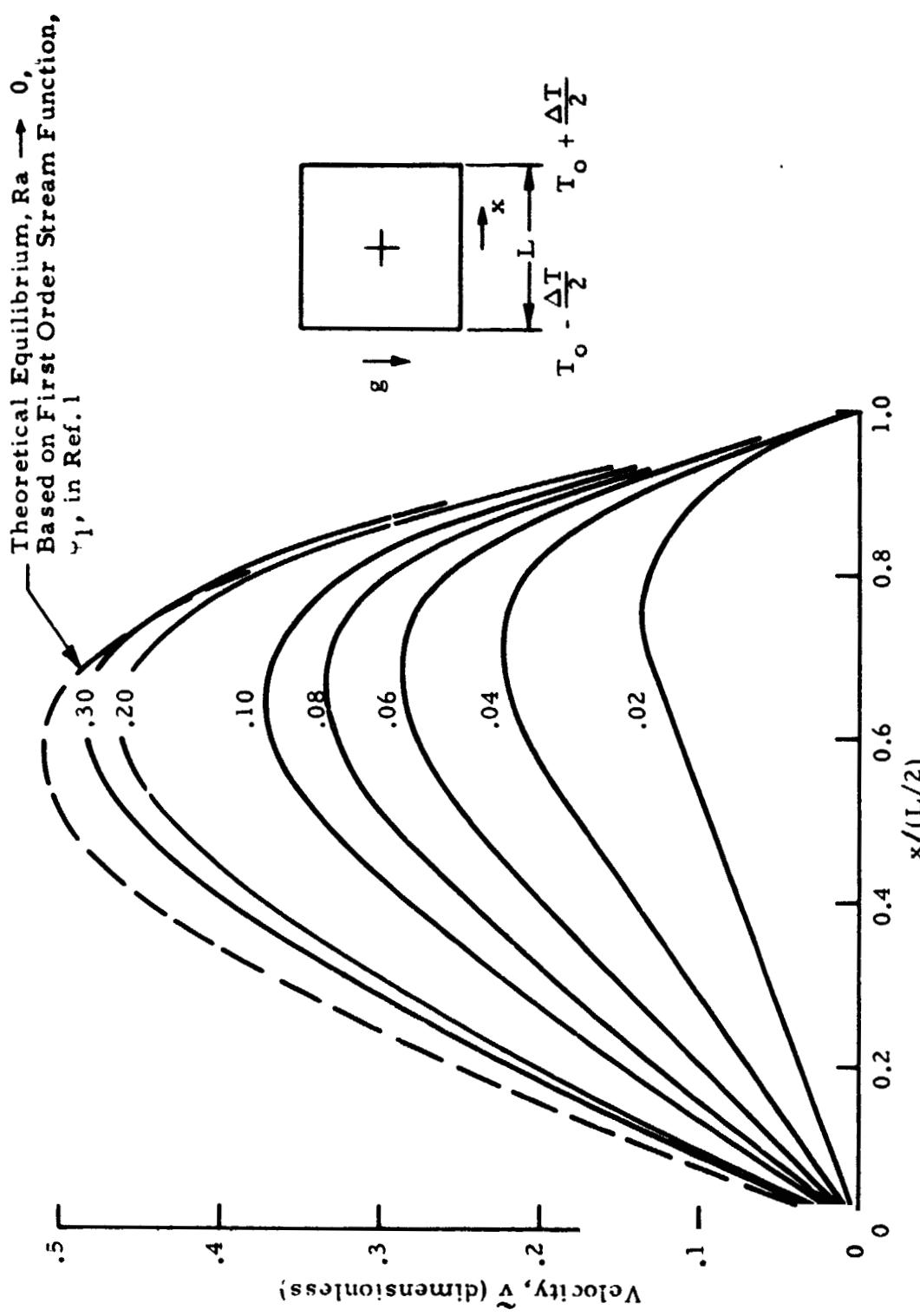
Fig. 19 - Velocity Distribution as a Function of Time for Water Contained in a Square Enclosure with Rayleigh Number = 1

27

Contour Labels same as Fig. 7

Temperature Contours

Velocity Vectors

$\tilde{t} = .1$

$\tilde{t} = .2$

$\tilde{t} = .3$

g
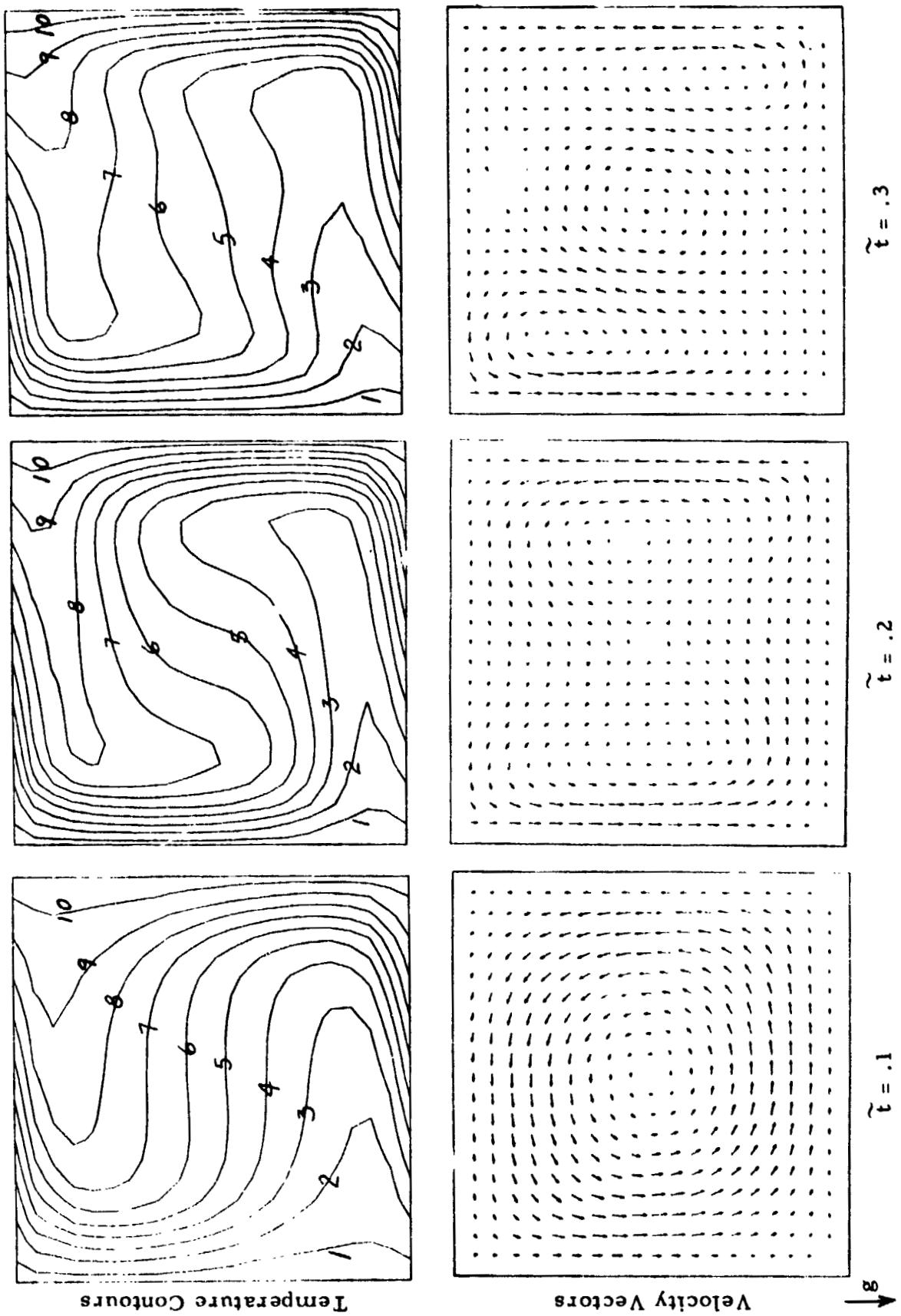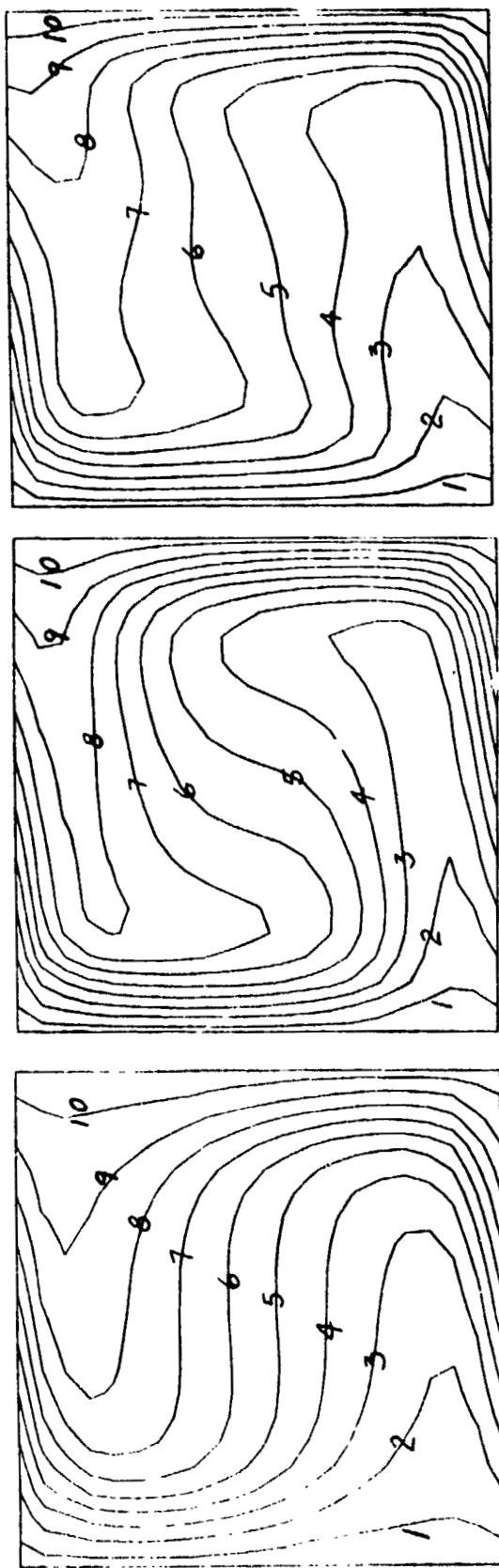
Fig. 20 - Comparison of GIM Code Temperature and Velocity Vector Variation with Time for Square Enclosure at Rayleigh Number of 100,000

$$.385 \frac{g \beta \Delta T \, d^2}{256 \, \nu} = .513 \frac{g \beta \Delta T \, L^2}{256 \, \nu}$$

$$d/L = 1.1543$$

Compare this ratio to the ratio 1.1284 that yields equal areas for the circle
and square. This somewhat fortuitous result clearly implies that an experi-
mental square enclosure may be closely modeled by a circular cylinder of
equal cross sectional area. The validity of this modeling is additionally
supported by the rather remarkable degree of radial symmetry that exists
in the low Rayleigh number velocity field in the square enclosure. This is
displayed in the angular variation of velocity shown in Fig. 21 for various
radial distances. These velocities were determined from the first order
stream function in Ref. 1.

LOCKHEED - HUNTSVILLE RESEARCH & ENGINEERING CENTER
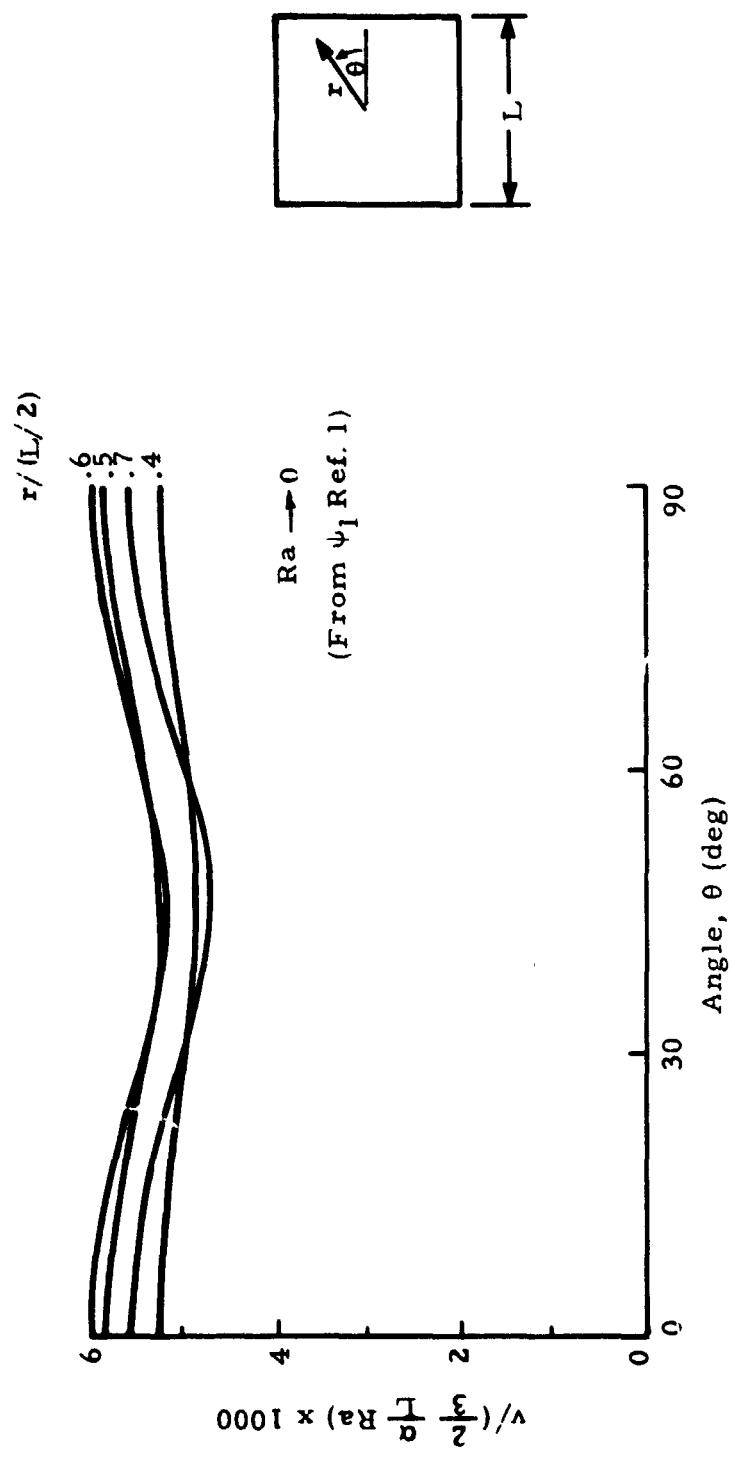
Fig. 21 Variation of Fluid Velocity with Angular Position Along Circular Arcs in Liquid Filled Square Container

4. CONCLUSIONS

The primary conclusion to be drawn from this study is that the low Rayleigh number theory for convection in circular cylinder and square box enclosures is valid throughout the transient phase to equilibrium for Rayleigh numbers up to at least 1000. The GIM code results, which we assume to be most valid, show a deviation of 20% from the low Rayleigh number results at Ra = 5,000. Additionally, for higher Rayleigh numbers, the low Rayleigh number theory is valid for some portion of the transient, depending on the value of the Rayleigh number, before significant deviation becomes apparent. In the case of both circular cylinder and square box enclosures at Ra = 100,000 the valid portion of the transient phase extends up to $\tilde{t} \cong 0.06$, which is approximately 20% of the time required to reach equilibrium.

Another conclusion drawn from the comparison of the circular cylinder and square box enclosure results is that experimental square shaped containers can be analytically modeled rather closely by circular cylinders of equal cross sectional area for the prediction of convection velocities and flow patterns at low Rayleigh number.

REFERENCES

1. Batchelor, G. W., "Heat Transfer by Free Convection Across a Closed Cavity Between Vertical Boundaries at Different Temperatures," Quart. Appl. Math., Vol. 12, No. 3, 1954, p. 209.

2. Weinbaum, S., "Natural Convection in a Horizontal Circular Cylinder," J. Fluid Mech., Vol. 18, 1964, p. 409.

3. Dressler, R. F., NASA Headquarters, Washington, D. C. (to be published).